




Quantum reflection of dark solitons scattered by reflectionless potential barrier and position-dependent dispersion

L. Al Sakkaf , T. Uthayakumar , and U. Al Khawaja **Department of Physics, United Arab Emirates University, P.O. Box 15551, Al-Ain, United Arab Emirates*

(Received 23 November 2021; revised 16 February 2022; accepted 20 May 2022; published 16 June 2022)

We investigate theoretically and numerically quantum reflection of dark solitons propagating through an external reflectionless potential barrier or in the presence of a position-dependent dispersion. We confirm that quantum reflection occurs in both cases with a sharp transition between complete reflection and complete transmission at a critical initial soliton speed. The critical speed is calculated numerically and analytically in terms of the soliton and potential parameters. Analytical expressions for the critical speed were derived using the exact trapped mode, time-independent, and time-dependent variational calculations. It is then shown that resonant scattering occurs at a critical speed, where the energy of the incoming soliton is resonant with that of a trapped mode. Reasonable agreement between analytical and numerical values for the critical speed is obtained as long as a periodic multisoliton ejection regime is avoided.

DOI: [10.1103/PhysRevE.105.064207](https://doi.org/10.1103/PhysRevE.105.064207)

I. INTRODUCTION

One of the fascinating phenomena observed for bright solitons in nonautonomous nonlinear systems is quantum reflection. In such a phenomenon, a soliton that approaches a potential can be reflected even in the absence of a classical turning point [1,2]. It portrays the wave nature of the soliton. Furthermore, such nonclassical interactions are known to exist only for the solitons approaching with lower velocities. However, if the incident soliton velocity is above a certain critical value, a sharp transition from complete reflection to complete transmission takes place. Subsequent investigations have revealed that such a feature results from the formation of a localized trapped-mode soliton at the center of the potential. Further, Ref. [3] obtained an accurate estimate of the critical speed by equating the energies of the incident soliton to that of the trapped mode. The same work also investigated the stability of the trapped modes against perturbations, for single-node as well as multinode trapped modes. The sharpness in the transition from complete reflection to complete transmission turns out to arise from the instability in the equilibrium position of the trapped-mode. Remarkably, investigations of such systems demonstrated the possibility of high-speed soliton ejection, even for stationary solitons positioned at a distance sufficiently far from the center of the potential. These higher ejection speeds are accompanied with multinode trapped modes that hold larger binding energy [4]. Quantum reflection of solitons is observed in diverse external potentials, for instance barriers [5–8], wells [1,2,9,10], steps [11,12], and surfaces [13–15]. Such studies allowed for an understanding of the energy exchange mechanism of the soliton during the scattering process with the potential to implement

soliton-based diodes, all-optical logic gates, switches, and filters using appropriate setups [16–21].

In general, quantum reflection of bright solitons through diverse potentials has been extensively analyzed. For instance, in optics, solitons are generated through compensating the group-velocity dispersion (GVD) with the Kerr nonlinearity during its evolution through an optical fiber. In view of nonlinear evolution with the negative GVD (anomalous dispersion), the fiber supports the pulse propagation in the form of a sech pulse profile, and such stable nonlinear pulses are universally acknowledged as a bright soliton [22–24]. For positive GVD (normal dispersion), the soliton manifests itself as a localized dip in the intensity with a uniform continuous-wave background. These dark solitons also possess the same shape- and velocity-preserving propagation as that of their bright counterparts [25–27]. Since the theoretical prediction in optical fibers by Hasegawa and Tappert [25] and the experimental realization by Emplit *et al.* [28], considerable research efforts have been made to understand the dynamics of dark solitons in various situations under diverse nonlinear regimes. In addition, they are observed to be generated without the threshold in the input pulse power [29]. Although dark solitons are primarily studied in autonomous systems, their dynamics in nonautonomous systems in particular has enabled us to understand the diverse real physical situations in which complex forces appear [27].

Considering quantum reflection in dark solitons, Cheng *et al.* demonstrated the quantum reflection in Bose-Einstein condensates with a potential barrier. This study discussed how the quantum reflection phenomenon is influenced by diverse factors such as the barrier height and width, the orientation angle of the dark soliton, and the initial displacement of the condensate cloud. The reflection probability is found to be sensitive to the initial orientation, and it also influences the excitation process during the condensate and barrier interaction [30]. A potential in the form of a boxlike trap was also

*Corresponding author: u.alkhawaja@uaeu.ac.ae

considered for the investigation of dark-soliton dynamics in a BEC at zero temperature. In such a setup, the soliton is found to propagate through the trap without any dissipation. However, dissipation was observed during the reflection from a wall with the emission of sound waves, resulting in a slight increase in the speed of the solitons. For the multiple oscillations and reflections inside the trap, the energy loss and the speed are found to increase significantly [31]. From studies of dark soliton scattering by a two-defect potential, one can infer that dark solitons cannot be trapped by two identical potential barriers. Moreover, interactions of dark solitons in such a setup are found to increase the speed of the soliton while traversing through the first barrier, which always enables us to overcome the second one. This suggested that the only possibility to realize the optical diode based on dark soliton scattering is through time-dependent potential barriers [32]. The temporal reflection of an optical pulse illustrated the possibility to control the properties of dark solitons through another weak probe pulse [33].

The scattering of composite dark-bright solitons through a fixed localized δ impurity has also been considered [34]. It was shown that such interaction excited different modes that result in the emergence of a dark-bright soliton with a distinct velocity. In addition, the study investigated the scattering regimes of reflection and transmission, as well as inelastic scattering behavior with complex internal mode excitations. Recently, Hansen *et al.* described the propagation properties of matter-wave solitons through localized scattering potentials. They identified the regimes over which solitons can behave as a wave or as a particle as a consequence of the interplay between dispersion and the attractive atomic interactions [35]. Although numerous investigations were reported for dark solitons scattering in BECs, there is no significant study involving quantum reflection of dark solitonic pulses through scattering by potential barriers. In most situations, dark solitons are dealt with and treated in the presence of a bright-soliton background [34,35].

In the present study, we consider the scattering dynamics of dark solitons propagated very far from the center of an external potential or a region of modulated dispersion in order to investigate the existence and characteristics of quantum reflection. The study has three main objectives: (i) to confirm the existence of quantum reflection and to identify the type of potentials (well or barrier) needed for it to occur; (ii) to investigate the characteristics of the quantum reflection phenomenon in terms of the main parameters of the system, including the potential strength and initial soliton size; and (iii) to calculate both analytically and numerically the critical soliton speed for quantum reflection. Furthermore, our numerical investigations will show that for certain parameter regimes, a stimulated periodic multi-dark-soliton ejection will be triggered upon the scattering. We begin with a derivation, which considers the exact solutions for both bright and dark solitons, that gives the necessary conditions required for quantum reflection of dark solitons. Our study shows that the occurrence of quantum reflection in dark solitons requires a potential in the form of a barrier, which is in contrast with the situation for bright solitons, where it should be a potential well. We analyze the scattering dynamics of dark solitons with two kinds of potential barrier settings: (i) an external potential

barrier, and (ii) a position-dependent dispersion profile in the form of Dirac δ , square well, sech, and sech^2 potential barriers. Here, the position-dependent dispersion serves as an effective potential for scattering.

We organize the rest of the paper as follows. In Sec. II, we describe the scattering system. Then, we derive the exact energy functionals of both bright and dark solitons using, in Sec. II A, the exact solution of the nonlinear Schrödinger equation (NLSE) and, in Sec. II B, a variational calculation. In Sec. III, we calculate the effective potentials in the presence of an external potential and an x -dependent dispersion. A discussion of the necessary conditions for quantum reflection and numerical investigations of the scattering dynamics are performed as well in this section. In Sec. IV, we use a time-dependent variational calculation to derive the equations of motion. Finally, we summarize and discuss our main findings in Sec. V.

II. ENERGY FUNCTIONAL OF THE FUNDAMENTAL SOLITONS

In this section, we calculate the energy functional for bright and dark solitons using the exact solutions of the NLSE. We use also a variational calculation with an appropriate trial function that leads to the exact energy functionals. The aim here is to establish the notation and the theoretical framework. One of the issues to settle at the outset is the divergence in the energy and norm of the dark soliton due to its finite background. This divergence is removed by shifting the intensity profile by its asymptotic value at infinity.

We recall the fundamental bright and dark soliton solutions supported by the well-known fundamental NLSE, given by [22–24]

$$i \frac{\partial}{\partial t} \psi(x, t) = -g_1 \frac{\partial^2}{\partial x^2} \psi(x, t) - g_2 |\psi(x, t)|^2 \psi(x, t), \quad (1)$$

where $\psi(x, t)$ is a complex function, and g_1, g_2 are arbitrary real constants representing the strength of dispersion and nonlinear terms, respectively. In nonlinear optics, the NLSE describes the propagation of pulses in nonlinear media. In such a context, the dispersion term corresponds to the group velocity dispersion, which, depending on the sign of g_1 , compresses or spreads out the pulse, while the nonlinear term corresponds to the Kerr effect, which describes the modulation of the refractive index of the medium as a response to the propagating light pulse intensity.

A. Exact energy calculations of the fundamental bright and dark solitons

In attractive nonlinear media ($g_2 > 0$) with normal dispersion ($g_1 > 0$), or, alternatively, in repulsive nonlinear media ($g_2 < 0$) with anomalous dispersion ($g_1 < 0$), such that for both cases $g_2/g_1 > 0$, the NLSE, Eq. (1), supports a movable bright soliton solution denoted by $\psi_B(x, t)$ and written as

$$\psi_B(x, t) = n \sqrt{\frac{g_2}{8g_1}} \text{sech} \left[\frac{g_2 n (x - x_0 - vt)}{4g_1} \right] \times e^{\frac{i}{16g_1} [(g_2^2 n^2 - 4v^2)t + 8v(x - x_0)]}, \quad (2)$$

with a finite intensity normalized to n ,

$$N_B = \int_{-\infty}^{\infty} |\psi_B(x, t)|^2 dx = n,$$

where x_0 and v are the initial position and speed of the soliton center. The energy of the bright soliton is given by the energy functional

$$\begin{aligned} E_B &= \int_{-\infty}^{\infty} \left[g_1 \left| \frac{\partial}{\partial x} \psi_B(x, t) \right|^2 - \frac{1}{2} g_2 |\psi_B(x, t)|^4 \right] dx \\ &= -\frac{g_2^2 n^3}{48 g_1} + \frac{nv^2}{4 g_1}. \end{aligned} \quad (3)$$

In the contrary case in which $g_2/g_1 < 0$, a movable dark soliton solution denoted by $\psi_D(x, t)$ exists and takes the following form:

$$\begin{aligned} \psi_D(x, t) &= n \sqrt{-\frac{g_2}{8g_1}} \tanh \left[-\frac{g_2 n (x - x_0 - vt)}{4g_1} \right] \\ &\times e^{-\frac{i}{8g_1} [(g_2^2 n^2 + 2v^2)t - 4v(x - x_0)]}, \end{aligned} \quad (4)$$

with a negative finite intensity normalized to $-n$,

$$N_D = \int_{-\infty}^{\infty} [|\psi_D(x, t)|^2 - \rho_\infty] dx = -n,$$

where $\rho_\infty = \lim_{x \rightarrow \pm\infty} |\psi_D(x, t)|^2 = -g_2 n^2 / (8g_1)$ is the background intensity. The shift was necessary to avoid the divergence in the integral. The negative sign of the dark soliton norm is interpreted as a negative ‘‘mass’’ of a holelike excitation. The negative value results from measuring the norm with respect to the finite background ρ_∞ . To calculate the energy functional of a dark soliton, a similar shift in intensity is needed in order to remove divergences. This can be performed by expressing $\psi_D(x, t)$ in terms of intensity and phase as

$$\psi_D(x, t) = \sqrt{\rho(x, t)} e^{i\phi(x, t)}. \quad (5)$$

Shifting the intensity as $\rho(x, t) \rightarrow \rho(x, t) - \rho_\infty$, the energy of the dark soliton then reads

$$\begin{aligned} E_D &= g_1 \int_{-\infty}^{\infty} \left[(\rho(x, t) - \rho_\infty) \left(\frac{\partial}{\partial x} \phi(x, t) \right)^2 \right. \\ &\quad \left. + \left(\frac{\partial \sqrt{(\rho(x, t) - \rho_\infty)}}{\partial x} \right)^2 \right] dx \\ &\quad - \frac{1}{2} g_2 \int_{-\infty}^{\infty} [\rho(x, t) - \rho_\infty]^2 dx. \end{aligned} \quad (6)$$

Substituting for the $\rho(x, t)$ and $\phi(x, t)$ that correspond to solution Eq. (4), the energy functional takes the explicit form

$$E_D = \frac{g_2^2 n^3}{48 g_1} - \frac{nv^2}{4 g_1}, \quad (7)$$

which is equal to $-E_B$.

B. Time-independent variational calculation for fundamental bright and dark solitons

Here, we establish a variational calculation that reproduces the exact energy of bright and dark solitons. We perform

a time-independent variational calculation using the trial functions

$$\psi_{B\text{var}} = \sqrt{\frac{n\alpha}{2}} \operatorname{sech}[\alpha(x - x_0)] e^{iv(x-x_0)}, \quad (8)$$

$$\psi_{D\text{var}} = \sqrt{\frac{n\alpha}{2}} \tanh[\alpha(x - x_0)] e^{iv(x-x_0)}. \quad (9)$$

Using these trial functions, the energy expressions of both bright and dark solitons take the form

$$E_{B\text{var}} = ng_1 v^2 - \frac{1}{6} n^2 g_2 \alpha + \frac{1}{3} ng_1 \alpha^2, \quad (10)$$

$$E_{D\text{var}} = -ng_1 v^2 - \frac{1}{6} n^2 g_2 \alpha - \frac{1}{3} ng_1 \alpha^2. \quad (11)$$

The above-mentioned intensity shift is applied here as well in order to obtain the dark soliton energy. The equilibrium value of the variational parameter is obtained by the condition $\partial E_{B\text{var}/D\text{var}}/\partial \alpha = 0$, which gives $\alpha = ng_2/(4g_1)$ for the bright soliton and $\alpha = -ng_2/(4g_1)$ for the dark soliton. Substituting back into Eqs. (10) and (11) gives the energy expressions attained from the exact solutions Eqs. (3) and (7) with the replacement: $v \rightarrow (8v)/(16g_1)$. An important difference between the bright soliton and dark soliton energy expressions should be noted. While the energy of the bright soliton has a minimum at the equilibrium value of α , the dark soliton energy has a maximum. This indicates the stability of the bright soliton and the instability of the dark soliton against shrinking or broadening of the soliton width.

III. NLSE WITH EXTERNAL POTENTIAL AND POSITION-DEPENDENT DISPERSION

In the presence of an external potential, $V(x)$, or x -dependent dispersion, $f(x)$, the scattering dynamics of solitons is governed by the following NLSE:

$$\begin{aligned} i \frac{\partial}{\partial t} \psi(x, t) &= -g_1 f(x) \frac{\partial^2}{\partial x^2} \psi(x, t) \\ &\quad - g_2 |\psi(x, t)|^2 \psi(x, t) + V(x) \psi(x, t), \end{aligned} \quad (12)$$

where $\psi(x, t)$ is the field describing the intensity of the soliton. For matter-wave solitons in Bose-Einstein condensates, it corresponds to the wave function of the condensate. For localized dispersion modulations, the x -dependent dispersion satisfies the boundary condition $\lim_{x \rightarrow \pm\infty} f(x) = 1$, which is guaranteed with the following form:

$$f(x) = 1 + \delta(x), \quad (13)$$

where $\delta(x)$ is a localized function over a zero background. Formally, a moving localized solution is written as

$$\psi(x, t) = \sqrt{\rho(x - x_0 - vt)} e^{iv(x-x_0)}. \quad (14)$$

The energy functional corresponding to Eq. (12) reads

$$\begin{aligned} E &= \int_{-\infty}^{\infty} \left[-g_1 f(x) \psi^*(x, t) \frac{\partial^2}{\partial x^2} \psi(x, t) \right. \\ &\quad \left. - \frac{1}{2} g_2 |\psi(x, t)|^4 + V(x) |\psi(x, t)|^2 \right] dx, \end{aligned} \quad (15)$$

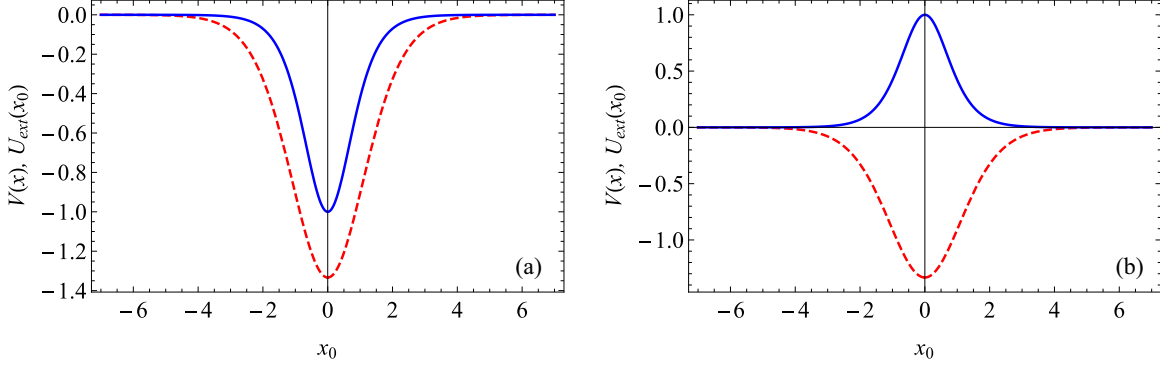


FIG. 1. External potentials and effective external potentials as given by Eqs. (25) and (26), (a) with a bright soliton, $g_2 = 1$, $V_0 = -1$; and (b) with a dark soliton, $g_2 = -1$, $V_0 = 1$. Solid blue and dashed red curves correspond to the external potential and effective potential, respectively. Parameters used are $g_1 = 1/2$, $n = 2$.

which takes the form

$$E = \int_{-\infty}^{\infty} \left[g_1 \left| \frac{\partial}{\partial x} \psi(x, t) \right|^2 - \frac{1}{2} g_2 |\psi(x, t)|^4 \right] dx + g_1 \int_{-\infty}^{\infty} \left[\delta(x) \left| \frac{\partial}{\partial x} \psi(x, t) \right|^2 + \delta'(x) \psi^*(x, t) \frac{\partial}{\partial x} \psi(x, t) \right] dx + \int_{-\infty}^{\infty} V(x) |\psi(x, t)|^2 dx, \quad (16)$$

where $(\cdot)'$ denotes a first derivative with respect to x , and $(\cdot)^*$ indicates complex conjugate. The first line in this equation is the energy of the fundamental soliton, the second and third lines correspond to the effective potentials resulting from the x -dependent dispersion and external potential, respectively. The energy is thus rewritten as

$$E(x_0, vt) = E_0 + U_{\text{disp}}(x_0, vt) + U_{\text{ext}}(x_0, vt), \quad (17)$$

which upon using the moving localized solution, Eq. (14), results in the following expressions:

$$E_0 = \int_{-\infty}^{\infty} \left[g_1 v^2 \rho(x - x_0 - vt) + g_1 \left(\frac{\partial \sqrt{\rho(x - x_0 - vt)}}{\partial x} \right)^2 - \frac{1}{2} g_2 \rho^2(x - x_0 - vt) \right] dx, \quad (18)$$

$$U_{\text{disp}}(x_0 + vt, v) = g_1 (v^2 I_1 + I_2 + iv I_3), \quad (19)$$

$$U_{\text{ext}}(x_0 + vt) = \int_{-\infty}^{\infty} V(x) \rho(x - x_0 - vt) dx, \quad (20)$$

with

$$I_1(x_0 + vt) = \int_{-\infty}^{\infty} \delta(x) \rho(x - x_0 - vt) dx, \quad (21)$$

$$I_2(x_0 + vt) = \int_{-\infty}^{\infty} \frac{\partial \sqrt{\rho(x - x_0 - vt)}}{\partial x} \left(\delta(x) \frac{\partial \sqrt{\rho(x - x_0 - vt)}}{\partial x} + \delta'(x) \sqrt{\rho(x - x_0 - vt)} \right) dx, \quad (22)$$

$$I_3(x_0 + vt) = \int_{-\infty}^{\infty} \delta'(x) \rho(x - x_0 - vt) dx. \quad (23)$$

An important consequence of the x -dependent dispersion is the non-Hermiticity of the Hamiltonian indicated by the

appearance of an imaginary part in the energy functional, $ivI_3(x_0 + vt)$. However, the effect of this non-Hermitian contribution is limited to the localized region of $\delta(x)$ where the scattering is taking place. At this region, the speed of the soliton is typically small, which makes the effect of this term insignificant. Therefore, it can be neglected during the whole evolution time. From another perspective, we are interested in calculating the effective potential for a nonmoving initial soliton, $v = 0$. Therefore, neither the first term nor the non-Hermitian term will contribute to U_{disp} . The effective potential will then be a function of only x_0 , as follows:

$$U_{\text{eff}}(x_0) \equiv E(x_0) = E_0 + U_{\text{disp}}(x_0) + U_{\text{ext}}(x_0). \quad (24)$$

Explicit formulas of U_{eff} will be obtained below by considering specific forms of $V(x)$ and $\delta(x)$ for both bright and dark solitons, where again the replacement $\rho(x - x_0 - vt) \rightarrow \rho(x - x_0 - vt) - \rho_\infty$ is required for the latter to avoid divergence. For bright solitons, we employ the solution Eq. (8), which gives $\rho(x, t) = (n\alpha/2) \text{sech}^2[\alpha(x - x_0)]$ and $\phi(x, t) = v(x - x_0)$. For the dark soliton, Eq. (9) gives $\rho(x, t) = (n\alpha/2) \tanh^2[\alpha(x - x_0)]$ and $\phi(x, t) = v(x - x_0)$, where the shifted intensity is $\rho(x, t) - n\alpha/2 = -(n\alpha/2) \text{sech}^2[\alpha(x - x_0)]$.

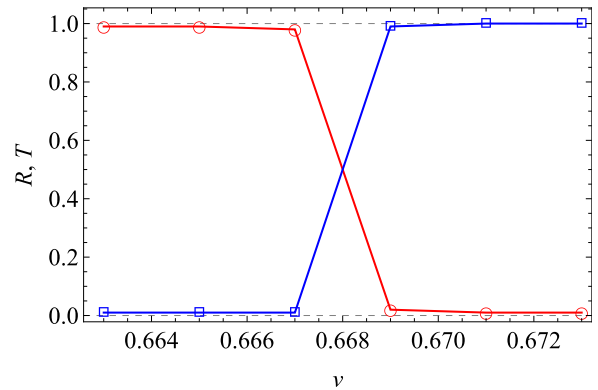


FIG. 2. Reflection (red circles) and transmission (blue squares) coefficients vs the initial speed of a dark soliton scattering by a reflectionless potential barrier, Eq. (25). Parameters used are $V_0 = 0.6$, $\alpha = \sqrt{V_0}$, $g_1 = 1/2$, $g_2 = -1$, $x_0 = -10$, and $n = 4$.

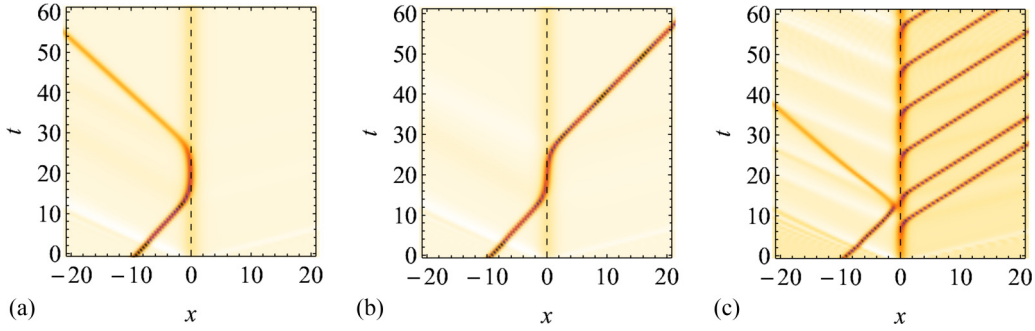


FIG. 3. Quantum scattering of the dark soliton [Eq. (4)] by an effective potential [Eq. (26)]. The center of the external potential is indicated by the vertical dashed line. (a) Quantum reflection with critical speed $v = v_c = 0.665$, (b) transmission with $v = 0.67$, and (c) multiejection $v = 0.8$, $V_0 = 2$. Other parameters used are the same as those in Fig. 2.

A. Effective external potential

For the scattering of dark solitons by an external potential, we consider the reflectionless Pöschl-Teller potential provided by

$$V(x) = V_0 \operatorname{sech}^2(\alpha x), \quad (25)$$

where V_0 and $\alpha = \sqrt{|V_0|}$ are the height and inverse width of the potential. The corresponding effective external potential can be obtained using Eq. (20) as

$$U_{\text{ext}}(x_0) = \pm 2nV_0[\alpha x_0 \coth(\alpha x_0) - 1] \operatorname{csch}^2(\alpha x_0), \quad (26)$$

where the positive and negative overall signs relate to the bright and dark solitons, respectively. This \pm prefactor leads to an important conclusion about how the effective potential $U_{\text{ext}}(x_0)$ relates to the actual external potential $V(x)$. For a bright soliton, the effective potential will be a barrier (well) if the external potential is a barrier (well), but for the dark soliton the effective potential is a barrier (well) if $V(x)$ is a well (barrier). In Fig. 1, this is shown clearly where we plot the effective potential Eq. (26) corresponding to the bright and dark solitons together with $V(x)$.

Quantum reflection takes place when the soliton is reflected by a region of effective potential well. Therefore, while quan-

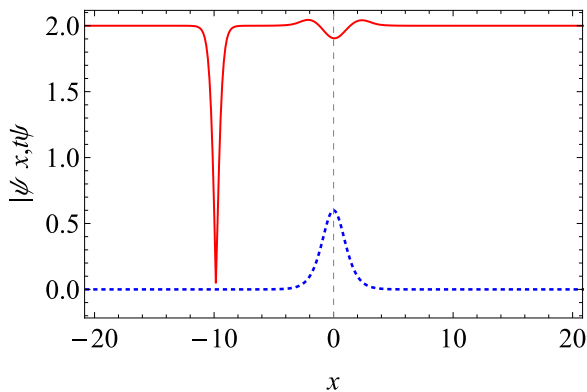


FIG. 4. Existence of a trapped mode at the center of the potential before the propagation. The dotted blue curve corresponds to the potential barrier, which behaves as an effective potential well. Parameters used are $V_0 = 0.6$, $\alpha = \sqrt{V_0}$, $g_1 = 1/2$, $g_2 = -1$, $n = 4$, $v = 0.51$.

tum reflection of bright solitons takes place with $V(x)$ being a potential well, the situation is reversed for dark solitons. Quantum reflection of dark solitons takes place when $V(x)$ is a potential barrier.

In the following two subsections, we investigate further the quantum reflection of a potential barrier both numerically and analytically. Specifically, we will show that, similar to bright solitons, a sharp transition between full transmission and full reflection takes place at a critical soliton speed. The physics of quantum reflection turns out also to be similar to that of the bright soliton case in which a trapped mode is formed at the potential. The critical speed for quantum reflection in terms of the strength of the potential V_0 will also be calculated using the numerical [36] and analytical approaches.

1. Calculation of the critical speed from the numerical solution of Eq. (12)

We solve numerically Eq. (12) in the presence of the external potential Eq. (25), where we set $\delta(x) = 0$ and use $\psi_D(x, 0)$ from Eq. (14) as an initial profile. We define the scattering coefficients as

$$R = (1/N_D) \int_{-\infty}^{-l} [|\psi_D(x, t_f)|^2 - \rho_\infty] dx, \quad (27)$$

$$T = (1/N_D) \int_l^{\infty} [|\psi_D(x, t_f)|^2 - \rho_\infty] dx, \quad (28)$$

where N_D is defined by Eq. (5), R and T are the scattering coefficients of reflection and transmission, respectively, l is a length larger than the width of the potential, and t_f is an evolution time such that the scattered soliton is sufficiently far from the potential. Figure 2 shows a clear possibility of obtaining quantum reflection where a sharp transmission of the coefficients from complete reflectance to complete transmittance is achieved at $v = 0.67$. This is confirmed by the spatiotemporal plots in Figs. 3(a) and 3(b), where the two different scattering outcomes are obtained for initial soliton speeds just below and above the critical speed. The excitation of a trapped mode is also verified in Fig. 4, where a snapshot shows a dark soliton at the potential center. Higher-energy trapped modes were also found for larger potential barrier strengths. However, in such a case, quantum reflections are found to be accompanied by a considerable amount of radiation, or even completely replaced by multisoliton ejections, as indicated by Fig. 3(c).

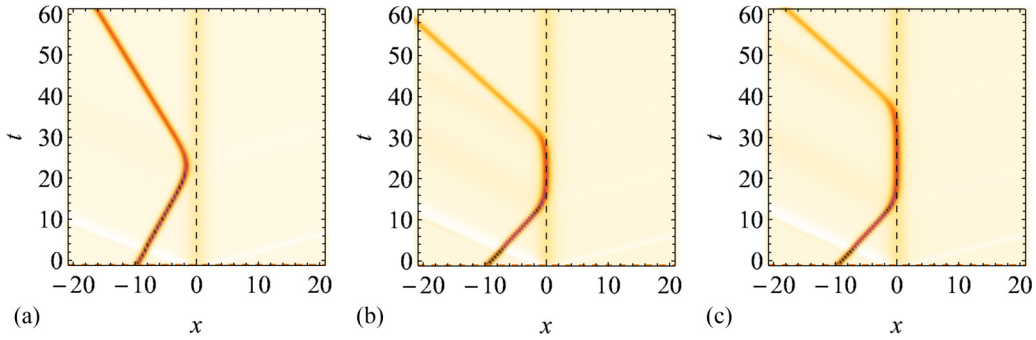


FIG. 5. Quantum reflection of the dark soliton Eq. (4) at different speeds by the potential Eq. (26) with barrier height $V_0 = 0.6$. The center of the external potential is indicated by the vertical dashed line. (a) $v = 0.4$, (b) $v = 0.66658$, and (c) $v = 0.666999$. Other parameters used are the same as those in Fig. 2.

In Fig. 5, we show the influence of the initial speed over the duration of the trapped mode. The duration of the trapped mode is increased with the initial speed of the soliton. It reaches the maximum length at the critical speed, before the soliton gets transmitted. Next, we consider the role of the potential barrier height on the trapped mode formation in Fig. 6. At a lower height of the potential barrier, we found a shift in the scattering outcomes, where it switches from the reflection to the transmission regime, as the required critical speed is lower for a lower barrier height.

The dependence of the critical speed for quantum reflection on the strength of the potential is shown by the solid blue curve in Fig. 7. For $V_0 > 1.1$, the scattering of dark solitons results in the above-mentioned multisoliton ejection behavior as illustrated in Fig. 3(c). Hence, we restricted ourselves to the goal of investigating quantum reflection, while multisoliton ejection will be considered for study in the near future.

2. Calculation of the critical speed with an exact trapped mode solution

Based on our understanding of the mechanism of quantum reflection, a trapped mode plays a crucial role in determining the sharp transition between full transmission and full (quantum) reflection. Simply, if the energy of the incoming soliton is larger (less) than the energy of the trapped mode, the soliton will be fully transmitted (reflected). If the energy of the incident soliton is equal to that of the trapped mode, the

soliton will be trapped, though such a trapped state is unstable against small perturbations in position or width of the soliton. Consequently, to account for the critical speed theoretically, it is essential to determine the properties of the trapped mode, mainly its profile and energy. Fortunately, an analytic exact solution, which is the nodeless trapped mode, exists for the NLSE with the reflectionless Pöschl-Teller potential. Here, we will exploit this solution to present an analytic derivation of the critical speed in terms of the potential strength, which will provide an independent account for our earlier numerical calculation with which we can compare.

In the absence of the x -dependent dispersion and with the presence of the Pöschl-Teller potential, $V(x) = V_0 \operatorname{sech}^2(\sqrt{V_0}x)$, the NLSE Eq. (12) with $g_1 = 1/2$, $g_2 < 0$, and $V_0 > 0$ admits the exact dark soliton solution

$$\psi_{\text{trap}}(x, t) = \sqrt{-\frac{2V_0}{g_2}} \tanh(\sqrt{V_0}x) e^{-2iV_0 t}, \quad (29)$$

which, upon substituting in the energy functional Eq. (17) with $U_{\text{disp}} = 0$ and taking into account the corresponding shifted intensity as $\rho(x, t) + 2V_0/g_2 = (2V_0/g_2) \operatorname{sech}^2(\sqrt{V_0}x)$, gives the exact trapped energy that takes the form

$$E_{\text{trap}} = \frac{2V_0^{3/2}}{3g_2}. \quad (30)$$

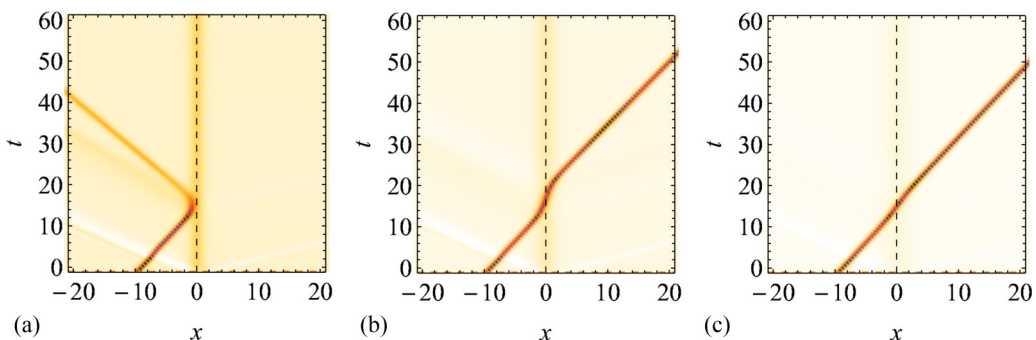


FIG. 6. Scattering of the dark soliton [Eq. (4)] at the critical speed $v_c = 0.665$ by an effective potential [Eq. (26)] with different barrier heights. The center of the external potential is indicated by the vertical dashed line. (a) $V_0 = 1$, (b) $V_0 = 0.5$, and (c) $V_0 = 0.2$. The rest of the parameters used are the same as in Fig. 2.

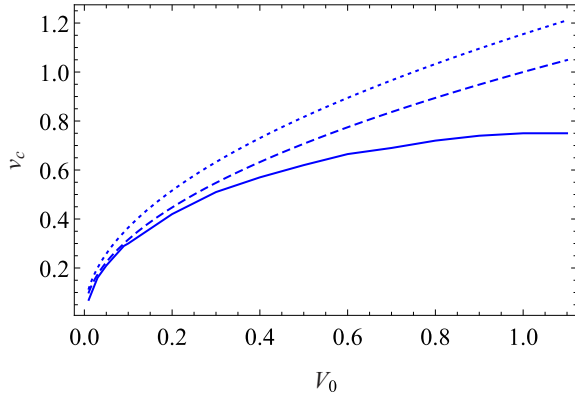


FIG. 7. Critical soliton speed, v_c , at which the dark soliton will be reflected by the effective potential Eq. (26) in terms of its strength, V_0 . The solid curve is obtained from the numerical solution of Eq. (12), as explained in the text. The dashed curve is the analytical result Eq. (32). The dotted curve is the result of time-dependent variational calculation Eq. (43). Parameters used are $\alpha = \sqrt{V_0}$, $g_1 = 1/2$, $g_2 = -1$, $x_0 = -10$, $n = 4$.

The initial profile of the soliton is taken as the exact dark soliton of the fundamental NLSE, namely Eq. (4), thus the energy of the initial soliton takes the form of Eq. (7). Equating the two energies in Eq. (7) and (30), $E_D = E_{\text{trap}}$, yields the exact critical speed for quantum reflection,

$$v_c = \sqrt{\frac{g_2^2 n^2}{12} - \frac{4V_0^{3/2}}{3ng_2}}. \quad (31)$$

In addition to equating their energies, the norms of the initial and trapped solitons should be equal. As given by Eq. (5), the norm of the initial soliton is $-n$. The norm of the trapped mode Eq. (29) is calculated to be $n = 4\sqrt{V_0}/g_2$. Equating the two norms and then substituting for n in Eq. (31), we get

$$v_c = \sqrt{V_0}. \quad (32)$$

This theoretical result agrees favorably with the numerical calculation, as shown by the dashed blue curve in Fig. 7, especially for smaller values of V_0 . As noted above, for larger values of V_0 , radiation increases. Keeping in mind that the theoretical calculation of v_c does not take into account radiated

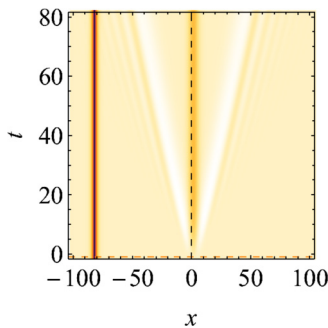


FIG. 8. Numerical experiment portraying the trapped mode soliton formed at the center of the potential barrier for a stationary dark soliton positioned at $x_0 = -80$. The center of the external potential is indicated by the vertical dashed line. Parameters used are $u_0 = 0.45$, $g_1 = 1/2$, $g_2 = -1$, $V_0 = 0.1$, $\alpha = \sqrt{V_0}$.

energy, this explains the increased deviation of the theoretical result from the numerical one.

Furthermore, it is observed that radiation is emitted during the population of the trapped mode even for a stationary dark soliton and irrespective of its initial position from the potential. One such trapped mode soliton appears at the center of the potential barrier, for an initial stationary dark soliton positioned at $x_0 = -80$, as displayed in Fig. 8. This trapped mode soliton is obtained for the initial dark soliton with an amplitude $u_0 = \sqrt{\frac{-2V_0}{g_2}} = 0.45$ using the parameter setting $V_0 = 0.1$, $g_1 = 0.5$, and $g_2 = -1$. Although the exact trapped mode soliton does not account for the radiation, we note that in real situations such interactions are featured with background radiation that appears on either side of the potential barrier. The emergence of such radiations is due to the continuous interaction between the background of the dark soliton with the potential barrier.

B. Effective position-dependent dispersion

As an alternative method of achieving quantum reflection with dark solitons, we consider a different approach that can induce the same effect of an external potential. This involves the scattering of a dark soliton by an x -dependent dispersion. Such x -dependent dispersion can be assumed as any of the following forms of $\delta(x)$:

$$\delta(x) = \begin{cases} U_0 \delta_{\text{Dirac}}(x/w), & (33a) \\ U_0 \times \begin{cases} 1, & |x| \leq w/2, \\ 0, & |x| > w/2, \end{cases} & (33b) \\ U_0 \text{sech}(\alpha x), & (33c) \\ U_0 \text{sech}^2(\alpha x), & (33d) \end{cases}$$

where U_0 and w are the strength and width of the localized dispersion, respectively, and $\alpha = \sqrt{|U_0|}$. The effective potentials corresponding to these dispersion functions for the bright and dark solitons are calculated using Eq. (19) as

$$U_{\text{disp}}(x_0, 0)$$

$$\begin{cases} \frac{g_1 n U_0 w \alpha^3 \text{sech}^4(\alpha x_0)}{4} [3 - \cosh(2\alpha x_0)], & (34a) \\ \frac{g_1 n U_0 \alpha^2}{6} \left\{ \tanh^3 \left[\frac{\alpha}{2} (w - 2x_0) \right] + \tanh^3 \left[\frac{\alpha}{2} (w + 2x_0) \right] \right\}, & (34b) \\ \pm \frac{g_1 n \pi U_0 \alpha^2}{8} \text{sech}^4 \left(\frac{\alpha x_0}{2} \right), & (34c) \\ \frac{g_1 n U_0 \alpha^2 x_0 \text{csch}^5(\alpha x_0)}{6} [27 \sinh(\alpha x_0) + 7 \sinh(3\alpha x_0) \\ - 45 \alpha \cosh(\alpha x_0) - 3\alpha \cosh(3\alpha x_0)], & (34d) \end{cases}$$

where in the third line, the $+$ sign relates to the effective potential for the bright soliton, and the $-$ sign corresponds to the dark soliton. For the other results, the effective potential is the same for both bright and dark solitons. In Fig. 9, we plot the effective dispersion potentials obtained above for both the bright and dark solitons. Since the profile of the effective dispersion corresponding to $\delta(x) = U_0 \text{sech}(\alpha x)$ has monotonically decaying tails without the appearance of secondary peaks besides the main peak, we choose to focus on this function through our investigations below. Additionally, pulse profiles featured with secondary peaks, other than the central peak, result in complex scattering dynamics and eventually lead to some further radiation during the numerical simulations. A similar analogy to the case with external potential

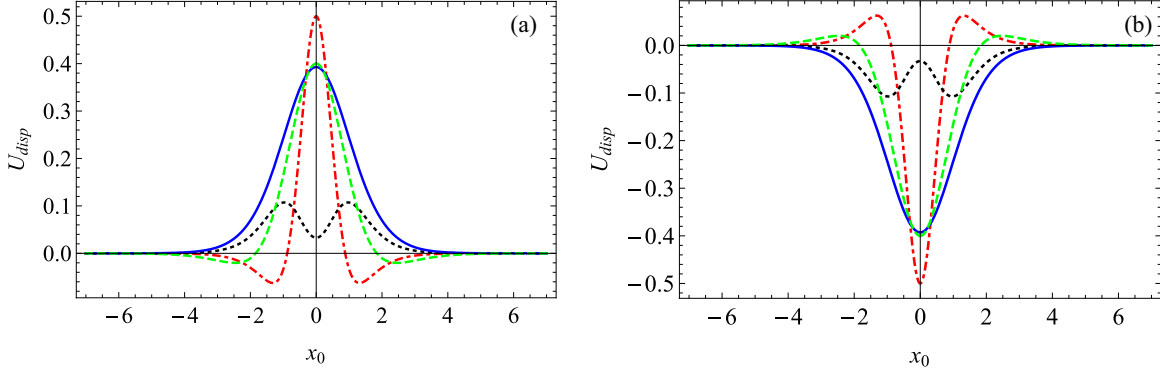


FIG. 9. Effective dispersion potentials for different x -dependent dispersion functions $\delta(x)$, as given by Eq. (33a). Dotted dashed red line: Eq. (34a); dotted black line: Eq. (34b); solid blue line: Eq. (34c); dashed green line: Eq. (34d). (a) With bright soliton, $g_2 = 1$, and (b) with dark soliton, $g_2 = -1$. Parameters used are $U_0 = 1$, $g_1 = 1/2$, $n = 2$, $w = 1$.

applies here; for dark solitons, quantum scattering requires the effective potential to be a well. Thus, quantum scattering can be achieved with the parameter set $g_1 > 0$, $g_2 < 0$, $U_0 > 0$, while the parameter set $g_1 > 0$, $g_2 < 0$, $U_0 < 0$ leads to the classical scattering regime.

In the following, we discuss the results obtained for quantum scattering parameters. We solve numerically Eq. (12) using the function Eq. (33c). We set $V(x) = 0$ and launch $\psi_D(x, 0)$ using Eq. (12) as an initial soliton. We defined the reflection and transmission coefficients by Eqs. (27) and (28), where in this situation l indicates the length larger than the width of the x -dependent dispersion. In Fig. 10, we plot the scattering coefficients versus the incident soliton speed. The figure clearly shows the possibility of obtaining quantum reflection, where a sharp transmission of the coefficients from full reflectance to full transmittance is achieved. This is confirmed by the spatiotemporal plots in Fig. 11. The critical speed for quantum reflection, v_c , is calculated numerically by running the initial soliton speed such that it gets trapped at the potential. In Fig. 12, we plot the critical speed versus U_0 . The dependence of v_c on U_0 is found to be similar to that of the dependence of v_c on V_0 for the external potential barrier case. Moreover, in Fig. 11(c), we show a multiejection behavior

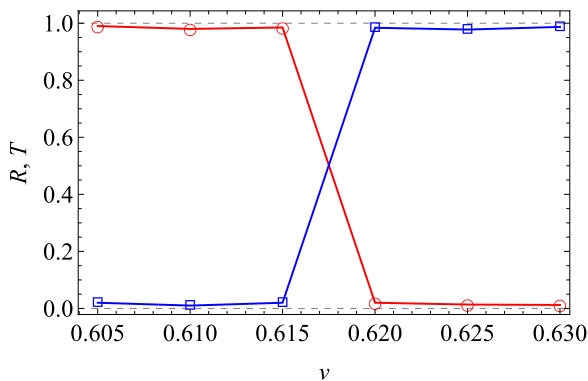


FIG. 10. Reflection (red circles) and transmission (blue squares) coefficients vs initial speed of a dark soliton scattering by an x -dependent dispersion Eq. (33c). Parameters used are $U_0 = 0.4$, $g_1 = 1/2$, $g_2 = -1$, $\alpha = \sqrt{g_1 U_0}$, $x_0 = -10$, $n = -4$.

for the larger values of U_0 , such as the one observed for the external potential barrier.

IV. SCATTERING DYNAMICS OF DARK SOLITONS USING TIME-DEPENDENT VARIATIONAL CALCULATIONS

In this section, we use a time-dependent variational calculation to obtain an analytical account of the dynamical evolution of the scattering soliton. The appearance of quantum reflection above a critical speed will then be confirmed. This will also provide analytical expressions of the critical speed for cases of both external potential and position-dependent dispersion.

We employ the trial function of the dark soliton in Eq. (9) with varying the soliton center and velocity in t and the use of the shifted intensity, namely $v \rightarrow v(t)$, $x_0 \rightarrow x_0(t)$, and $\rho(x, t) = -(n\alpha/2) \text{sech}^2[\alpha(x - x_0(t))]$.

The Lagrangian function corresponding to the NLSE, Eq. (12), then takes the form

$$\begin{aligned} L &= \int_{-\infty}^{\infty} i\psi^*(x, t)\psi_t(x, t)dx - \int_{-\infty}^{\infty} \left[g_1 |\psi_x(x, t)|^2 \right. \\ &\quad \left. - \frac{1}{2} g_2 |\psi(x, t)|^4 + V(x) |\psi(x, t)|^2 \right] dx \\ &= \int_{-\infty}^{\infty} i\psi^*(x, t)\psi_t(x, t)dx \\ &\quad - [E_0 + U_{\text{disp}}(x_0, v) + U_{\text{ext}}(x_0, v)], \end{aligned} \quad (35)$$

where we have hidden the t -dependence for convenience.

A. Effective external potential well

In the presence of an external potential barrier and with the absence of the x -dependent dispersion, $V(x) = V_0 \text{sech}^2(\alpha x)$, $\delta(x) = 0$, the calculated Lagrangian in Eq. (35) with the trial function of the dark soliton, Eq. (9), takes the form

$$\begin{aligned} L &= -nvx_0 - \left\{ -\frac{1}{3} g_1 n(\alpha^2 + 3v^2) - \frac{1}{6} g_2 n^2 \alpha \right. \\ &\quad \left. - 2nV_0 \text{csch}^2(\alpha x_0) [\alpha x_0 \coth(\alpha x_0) - 1] \right\}. \end{aligned} \quad (36)$$

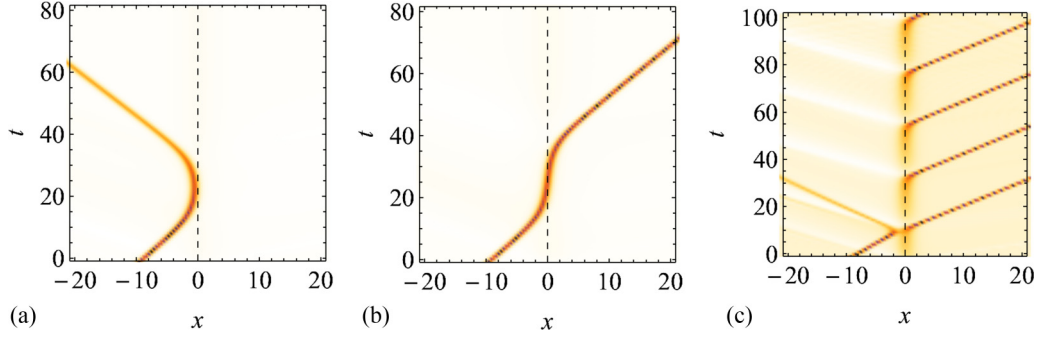


FIG. 11. Quantum scattering of the dark soliton Eq. (4) by an x -dependent dispersion Eq. (33c). The center of the x -dependent dispersion is indicated by the vertical dashed line. (a) Quantum reflection with critical speed $v = v_c = 0.615$, (b) transmission with $v = 0.62$, and (c) multiejection $v = 0.8$, $U_0 = 2$. Parameters used are the same as those in Fig. 10.

The corresponding Euler-Lagrange equations yield the following two equations of motion for the soliton center and velocity:

$$\dot{x}_0 - 2g_1v = 0, \quad (37)$$

$$-n\dot{v} - 6nV_0\alpha\coth(\alpha x_0)\operatorname{csch}^2(\alpha x_0) + 2V_0\alpha^2x_0(t)\operatorname{csch}^4(\alpha x_0)[2 + \cosh(2\alpha x_0)] = 0. \quad (38)$$

Integrating the above equation with respect to x_0 results in

$$-2nV_0\operatorname{csch}^2(x_0)[\alpha\coth(\alpha x_0)x_0 - 1] - \frac{1}{2}nv^2 - c = 0, \quad (39)$$

where c is the constant of integration.

For an initial position, $x_0(0)$, that is sufficiently far from the influence of the potential $V(x)$, the constant of integration can be calculated as

$$c = \frac{-nv_c^2}{2}, \quad (40)$$

where $v_c = v(0)$.

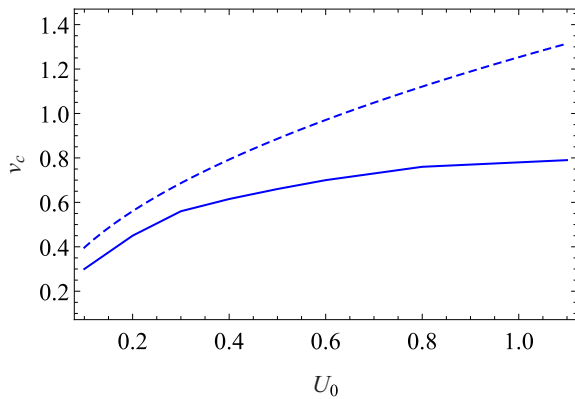


FIG. 12. Critical soliton speed, v_c , at which the dark soliton will be reflected by the x -dependent dispersion Eq. (33c) in terms of its height, U_0 . The solid curve is obtained from the numerical solution of Eq. (12), as explained in the text. The dashed curve is the result of time-dependent variational calculation Eq. (47). Parameters used are $g_1 = 1/2$, $g_2 = -1$, $\alpha = \sqrt{g_1U_0}$, $x_0 = -10$, $n = 4$.

Substituting the obtained constant of integration in Eq. (39) leads to

$$-2nV_0\operatorname{csch}^2(x_0)[\alpha x_0\coth(\alpha x_0) - 1] + \frac{1}{2}n(v^2 - v_c^2) = 0. \quad (41)$$

At the turning point that takes place at $t = t_c$, the velocity of the dark soliton vanishes, $v(t_c) = 0$, and thus v_c can be calculated from the preceding equation as

$$v_c = -2\sqrt{V_0(\sqrt{\{x_0(0)\alpha\coth[x_0(0)\alpha] - 1\}}\operatorname{csch}[x_0(0)\alpha]}. \quad (42)$$

The turning point position, $x_0(0)$, can be calculated from Eq. (38) by setting the effective force to zero, namely $n\dot{v} = 0$, which gives the solution $x_0(0) = 0$. Direct substitution of $x_0(0) = 0$ in the preceding equation leads to an undefined quantity. However, expanding it in powers of $x_0(0)$ and then taking the limit $x_0(0) \rightarrow 0$ shows that all terms except the zeroth-order one vanish, and the result becomes

$$v_c = 2\sqrt{\frac{V_0}{3}}. \quad (43)$$

This result is plotted by the dotted blue curve in Fig. 7. While good agreement is obtained with the numerical values for smaller barrier heights, V_0 , the deviation increases for larger barrier heights. The discrepancy is primarily due to not accounting for radiation and multiejection in the present variational approach.

In Fig. 13, we display the time-varying position and speed obtained from the solutions of the equations of motion Eqs. (37) and (38), which clearly show a sharp transition from full reflection to full transmission.

B. Effective well with position-dependent dispersion

In the presence of position-dependent dispersion given by $\delta(x) = U_0 \operatorname{sech}(\alpha x)$ and with $V(x) = 0$, the calculated Lagrangian in Eq. (35) with the trial function of the dark soliton, Eq. (9), is reduced to

$$L = -nv\dot{x}_0 - g_1 \left[-\frac{1}{3}n\alpha^2 - \frac{\pi}{4}nU_0v^2\operatorname{sech}^2\left(\frac{1}{2}\alpha x_0\right) - \frac{\pi}{8}nU_0\alpha^2\operatorname{sech}^4\left(\frac{1}{2}\alpha x_0\right) - nv^2 - \frac{1}{6g_1}g_2n^2\alpha \right], \quad (44)$$

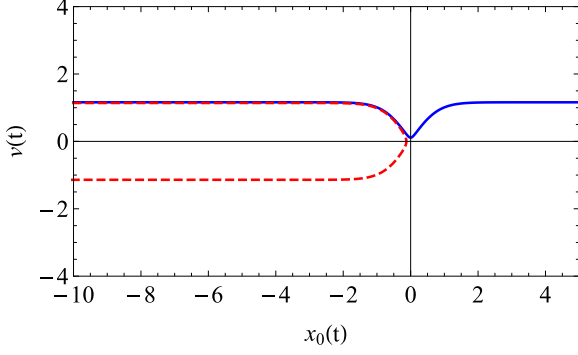


FIG. 13. Dynamics of the variational parameters, speed $v(t)$ vs position $x_0(t)$, corresponding to NLSE with external potential, Eqs. (37) and (38). Sharp reflection (dashed red) occurs at the critical speed $v = v_c = 1.15$ and transmission (blue) occurs at $v = 1.156$. Parameters used are $V_0 = 1$, $g_1 = 1/2$, $g_2 = -1$, $n = 4$.

where, based on our earlier discussion, we have neglected the non-Hermitian term. The Euler-Lagrange equations yield the following two equations of motion for the soliton center and velocity:

$$n\dot{x}_0 - 2g_1nv - \frac{\pi}{2}g_1nvU_0\text{sech}^2\left(\frac{1}{2}\alpha x_0\right) = 0, \quad (45)$$

$$-n\dot{v} + \frac{\pi}{4}g_1n\alpha U_0\text{sech}^2\left(\frac{1}{2}\alpha x_0\right)\tanh\left(\frac{1}{2}\alpha x_0\right) \times \left[v^2 + \alpha^2\text{sech}^2\left(\frac{1}{2}\alpha x_0\right)\right] = 0. \quad (46)$$

Following the derivation of the v_c expression Eq. (43) in the previous section, we obtain the critical speed for the present case,

$$v_c = \frac{1}{2}\alpha\sqrt{\pi g_1 U_0}. \quad (47)$$

The comparative results for v_c obtained through the Lagrangian approach and those through numerical simulations are shown in Fig. 12. Similar to the previous case, deviation of the variational values from the numerical ones increases with increasing U_0 , which, as we explained above, is due to not accounting for radiation. The trajectory in this case turns out to be very similar to that in Fig. 13, confirming the critical scattering behavior.

V. CONCLUSIONS AND OUTLOOK

We have considered quantum reflection of dark solitons in two setups: (i) in the presence of external potentials, and (ii) in the presence of an x -dependent dispersion. At the outset, we revisited the energy calculations and normalization of both bright and dark solitons in order to determine the energy functional and the condition that is necessary for quantum reflection to occur with dark solitons. Both analytical and variational calculations have shown that for quantum reflection of dark solitons to occur in the aforementioned setups, the actual external potential or dispersion modulation needs to be a barrierlike function that leads to an effective potential well in both cases.

To investigate the scattering dynamics, we derived the effective external potential corresponding to an external potential and an x -dependent dispersion using a suitable trial function for the dark soliton pulse. In the presence of an external potential, we considered the reflectionless Pöschl-Teller potential, and for the x -dependent dispersion we used the “sech” function, due to its corresponding effective potential without secondary peaks. This is followed by the numerical and analytical study of the soliton scattering.

Through our numerical investigations, we have observed quantum reflection for dark solitons for both settings considered. The critical speed required for such a phenomenon tends to increase with the height of the barrier. Moreover, our study revealed a transition regime from clear quantum reflection to a multiejection behavior for larger barrier heights. Analytical calculation of the critical speed in the case of an external potential was also possible using the exact trapped mode profile of the dark soliton scattered by a reflectionless potential barrier.

We have derived the dependence of the critical speed on the strength of the potential or dispersion modulation using variational calculations. The variational study has successfully shown the sharp transition behavior from full reflection to full transmission at the critical speed. The critical speed was calculated using three independent methods. The first method uses the exact trapped mode, the second employs a variational calculation, and the third is a numerical calculation. All three methods show that the critical speed increases with potential strengths. While the inclusion of radiation complicates the calculations, we believe it is worth investigating in a future work, as this will result in an accurate analytical formula that predicts the threshold of quantum reflection.

The critical speed of the dark soliton in real units can be estimated by transforming the Gross-Pitaevskii equation with the harmonic potential $V(x) = 1/2 m \omega^2 x^2$ into the dimensionless NLSE with a quadratic external potential. This transformation takes place with rescaling the position, x , and the time, t , as $x \rightarrow x/a$ and $t \rightarrow t\omega$, where $a = \hbar/(m\omega)$ is the harmonic trap width and ω is the trap frequency in the longitudinal direction. The speed is then given in terms of $v = a\omega$. For the case of repulsive ^{87}Rb condensate [37], $a = 109 a_0$ and $\omega = 674.20 \text{ s}^{-1}$, where $a_0 = 0.529 \times 10^{-10} \text{ m}$ is the Bohr radius. Therefore, the speed v will be determined in terms of $a\omega = 3.887 \times 10^{-6} \text{ m/s}$.

The above study is fully oriented to the quantum reflection, but in general such soliton scattering may lead to many other interesting phenomena, such as multiejection, snake trapping, and tree-ejection, which can be achieved by controlling the system parameters. In particular, we have noticed a region in the parameters space where periodic ejection of dark solitons is stimulated by the scattering. Further investigation of this behavior will be considered in the near future.

ACKNOWLEDGMENTS

The authors acknowledge the support of UAE University through Grants No. UAUEU-UPAR(1)-2019 and No. UAUEU-UPAR(11)-2019.

- [1] C. Lee and J. Brand, *Europhys. Lett.* **73**, 321 (2006).
- [2] T. Ernst and J. Brand, *Phys. Rev. A* **81**, 033614 (2010).
- [3] U. Al Khawaja, *Phys. Rev. E* **103**, 062202 (2021).
- [4] T. Uthayakumar, L. Al Sakkaf, and U. Al Khawaja, *Phys. Rev. E* **104**, 034203 (2021).
- [5] H. Sakaguchi and M. Tamura, *J. Phys. Soc. Jpn.* **74**, 292 (2005).
- [6] C. Weiss and Y. Castin, *Phys. Rev. Lett.* **102**, 010403 (2009).
- [7] O. V. Marchukov, B. A. Malomed, V. A. Yurovsky, M. Olshanii, V. Dunjko, and R. G. Hulet, *Phys. Rev. A* **99**, 063623 (2019).
- [8] V. Dunjko and M. Olshanii, [arXiv:1501.00075](https://arxiv.org/abs/1501.00075).
- [9] A. E. Miroshnichenko, S. Flach, and B. Malomed, *Chaos* **13**, 874 (2003).
- [10] K. T. Stoychev, M. T. Primatarowa, and R. S. Kamburova, *Phys. Rev. E* **70**, 066622 (2004).
- [11] M. Lizunova and O. Gamayun, [arXiv:2010.03385](https://arxiv.org/abs/2010.03385).
- [12] Y. Nogami and F. M. Toyama, *Phys. Lett. A* **184**, 245 (1994).
- [13] F. Baronio, C. De Angelis, P. Pioger, V. Couderc, and A. Barthélémy, *Opt. Lett.* **29**, 986 (2004).
- [14] H. Friedrich and J. Trost, *Phys. Rep.* **397**, 359 (2004).
- [15] R. Coté, H. Friedrich, and J. Trost, *Phys. Rev. A* **56**, 1781 (1997).
- [16] M. Asad-uz-zaman and U. Al Khawaja, *Europhys. Lett.* **101**, 50008 (2013).
- [17] U. Al Khawaja, S. M. Al-Marzoug, H. Bahlouli, and Y. S. Kivshar, *Phys. Rev. A* **88**, 023830 (2013).
- [18] M. O. D. Alotaibi, S. M. Al-Marzoug, H. Bahlouli, and U. A. Khawaja, *Phys. Rev. E* **100**, 042213 (2019).
- [19] U. Al Khawaja and A. A. Sukhorukov, *Opt. Lett.* **40**, 2719 (2015).
- [20] U. Al Khawaja, S. M. Al-Marzoug, and H. Bahlouli, *Phys. Lett. A* **384**, 126625 (2020).
- [21] A. Javed, T. Uthayakumar, M. O. D. Alotaibi, S. M. Al-Marzoug, H. Bahlouli, and U. Al Khawaja, *Commun. Nonlin. Sci. Numer. Simul.* **103**, 105968 (2021).
- [22] G. P. Agrawal, *Nonlinear Fiber Optics* (Academic, New York, 2013).
- [23] G. P. Agrawal, *Fiber-Optic Communication Systems* (Wiley, New York, 2010).
- [24] U. Al Khawaja and L. Al Sakkaf, *Handbook of Exact Solutions to the Nonlinear Schrödinger Equations* (IOP, London, 2020).
- [25] A. Hasegawa and F. Tappert, *Appl. Phys. Lett.* **23**, 171 (1973).
- [26] D. Krökel, N. J. Halas, G. Giuliani, and D. Grischkowsky, *Phys. Rev. Lett.* **60**, 29 (1988).
- [27] Y. S. Kivshar and B. Luther-Davies, *Phys. Rep.* **298**, 81 (1998).
- [28] P. Emplit, J. P. Hamaide, F. Reynaud, C. Froehly, and A. Barthélémy, *Opt. Commun.* **62**, 374 (1987).
- [29] S. A. Gredeskul and Yu. S. Kivshar, *Opt. Lett.* **14**, 1281 (1989).
- [30] Q. Cheng, W. Bai, Y. Zhang, B. Xiong, and T. Yang, *Laser Phys.* **29**, 015501 (2019).
- [31] M. Sciacca, C. F. Barenghi, and N. G. Parker, *Phys. Rev. A* **95**, 013628 (2017).
- [32] F. Tsitoura, Z. A. Anastassi, J. L. Marzuola, P. G. Kevrekidis, and D. J. Frantzeskakis, *Phys. Lett. A* **381**, 2514 (2017).
- [33] Z. Deng, Y. Chen, J. Liu, C. Zhao, and D. Fan, *Opt. Lett.* **43**, 5327 (2018).
- [34] M. O. D. Alotaibi and L. D. Carr, *J. Phys. B* **52**, 165301 (2019).
- [35] S. D. Hansen, N. Nygaard, and K. Mølmer, *Appl. Sci.* **11**, 2294 (2021).
- [36] U. Al Khawaja and Q. M. Al-Mdallal, *Int. J. Diff. Eq.* **2018**, 6043936 (2018); L. Al Sakkaf, Q. M. Al-Mdallal, and U. Al Khawaja, *Complexity* **2018**, 8269541 (2018); L. Al Sakkaf and U. Al Khawaja, *Alex. Eng. J* **61**, 11803 (2022).
- [37] J. Rogel-Salazar, *Eur. J. Phys.* **34**, 247 (2013).